# Influence of Covalent Character on High Li Ion Conductivity in a Perovskite-Type Li Ion Conductor: Prediction from a Molecular Dynamics Simulation of $La_{0.6}Li_{0.2}TiO_3$

Tetsuhiro Katsumata,*,† Yoshiyuki Inaguma,† Mitsuru Itoh,‡ and Katsuyuki Kawamura§

*Faculty of Science, Gakushuin University, 1-5-1 Mejiro, Toshima-ku, Tokyo 171-8588, Japan, Materials and Structures Laboratory, Tokyo Institute of Technology, 4259 Nagatsuta, Midori-ku, Yokohama 226-8503, Japan, and Faculty of Science, Tokyo Institute of Technology, 2-12-1, Ookayama, Meguro-ku, Tokyo 152-8551, Japan*

*Received April 17, 2002. Revised Manuscript Received July 8, 2002*

We executed a molecular dynamics simulation for the perovskite-type high Li ion conductor, $La_{0.6}Li_{0.2}TiO_3$, using two different potential models, the fully ionic model (FIM) and the partially ionic model (PIM). Good reproducibility of the physical properties was obtained for the simulation using the PIM. While displacement of the Li ion from the A-site was indicated in both models, Li ion diffusion was observed only for the PIM below 600 K. These results suggest that the introduction of a small mobile ion into the A-site does not always induce high ion conduction and that the covalent character of the Ti−O bond is indispensable to the high Li ion conduction. The ionic conductivity, however, could not reproduce quantitatively in this simulation due to the random distribution of A-site ions in the simulation cell.

## Introduction

The A-site-deficient perovskite-type oxide, $La_{2/3-x}Li_{3x}TiO_3$, shows high Li ion conductivity.[1,2] In this compound, La, Li, and vacancy are distributed in the A-site, and Li ions migrate through the conduction path composed of Li and vacancies. When the concentrations of Li ions and vacancies are optimized, that is, $La_{0.55}Li_{0.35}TiO_3$, the Li ion conductivity of the bulk part reaches $10^{-3}$ S/cm at room temperature, representing one of the highest values in solid Li ion conductors.[2] Recently, various studies of the transport mechanism have been carried out for these compounds, and it has been found that the valence of B-site ions influences the Li ion conduction.[3−19]

Itoh et al. have investigated the variations in Li ion conductivity with the lattice parameter for $Ln_{0.5}Li_{0.5}TiO_3$ (Ln = La, Pr, Nd, Sm).[3] They have found the ionic conductivity to decrease with the lattice parameter and the activation energy of the Li ion conduction to decrease linearly with decreases in the lattice parameter. Inaguma et al. have compared the dependence of the activation energy on the lattice parameter for various perovskite-type Li ion conductors.[5] Their results include data that can be divided into two groups: one group is composed of compounds containing only the Ti ion as a B-site ion, while the other group is composed of compounds containing Ti, Nb, and Ta ions as B-site ions. While the activation energy was found to increase

* To whom correspondence should be addressed. Tel.: +81-3-3986-0221. Fax: +81-3-5992-1029. E-mail: tetsuhiro.katsumata@gakushuin.ac.jp.

† Gakushuin University.

‡ Materials and Structures Laboratory, Tokyo Institute of Technology.

§ Faculty of Science, Tokyo Institute of Technology.

(1) Belous, A. G.; Novitiskaya, G. N.; Polyanetskaya, S. V.; Gornikov, Y. I. *Izv. Akad. Nauk SSSR, Neorg. Mater.* **1987**, *23*, 470−472.

(2) Inaguma, Y.; Chen, L.; Itoh, M.; Nakamura, T.; Uchida, T.; Ikuta, M.; Wakihara, M. *Solid State Commun.* **1993**, *86*, 689−693.

(3) Itoh, M.; Inaguma, Y.; Jung, W. H.; Chen, L.; Nakamura, T. *Solid State Ionics* **1994**, *70/71*, 203−207.

(4) Oguni, M.; Inaguma, Y.; Itoh, M.; Nakamura, T. *Solid State Commun.* **1994**, *91*, 624−630.

(5) Inaguma, Y.; Matsui, Y.; Yu, J.; Itoh, M. *Mater. Res. Soc. Symp. Proc.* **1997**, *453*, 623−628.

(6) Inaguma, Y.; Chen, L.; Itoh, M.; Nakamura, T. *Solid State Ionics* **1994**, *70/71*, 196−202.

(7) Katsumata, T.; Inaguma, Y.; Itoh, M. *Solid State Ionics* **1996**, *86−88*, 165−169.

(8) Léon, C.; Lucía, M. L.; Santamaría, J.; París, M. A.; Sanz, J.; Váres, A. *Phys. Rev. B* **1996**, *54*, 184−189.

(9) Inaguma, Y.; Itoh, M. *Solid State Ionics* **1996**, *86−88*, 257−260.

(10) Inaguma, Y.; Matsui, Y.; Yu, J.; Shan, Y. J.; Itoh, M.; Nakamura, T. *J. Phys. Chem. Solids* **1997**, *58*, 843−52.

(11) Léon, C.; Santamaría, J.; París, M. A.; Sanz, J.; Ibarra, J.; Torres, L. M.; Váres, A. *Phys. Rev. B* **1997**, *56*, 5302−05.

(12) Lee, J. S.; Yoo, K. W.; Kim, T. S.; Jung, H. J. *Solid State Ionics* **1997**, *98*, 15−26.

(13) Emery, J.; Buzare, J. Y.; Bohnke, O.; Fourquet, J. L. *Solid State Ionics* **1997**, *99*, 41−51.

(14) Birke, P.; Scharner, S.; Huggins, R. A. *J. Electrochem. Soc.* **1997**, *144*, L167−169.

(15) Léon, C.; Lucía, M. L.; Santamaría, J.; Sánches-Quesada, F. *Phys. Rev. B* **1998**, *57*, 41−47.

(16) Katsumata, T.; Inaguma, Y.; Itoh, M.; Kawamura, K. *J. Ceram. Soc. Jpn.* **1999**, *107*, 615−621.

(17) Harada, Y.; Watanabe, H.; Kuwano, J.; Saito, Y. *J. Power Sources* **1999**, *81−82*, 777−781.

(18) París, M. A.; Sanz, J.; Léon, C.; Santamaría, J.; Ibarra, J.; Váres, A.; *Chem. Mater.* **2000**, *12*, 1694−1701.

(19) Léon, C.; Rivera, A.; Váres, A.; Sanz, J.; Santamaría, J.; Ngai, K. L.; *Phys. Rev. Lett.* **2001**, *86*, 1279−1282.

10.1021/cm0203969 CCC: $22.00 
Published on Web 08/09/2002

linearly with decreases in the lattice parameter for both groups, the activation energy in the latter group is higher than that in the former group when these compounds have the same lattice parameter. These results suggest that to obtain the same activation energy in a compound containing a pentavalent cation in the B-site as that of a compound containing only the Ti ion in the B-site, a larger lattice parameter is required for the former compound. Furthermore, Harada et al. have prepared many perovskite-type Li ion conductors and have investigated the relationship between ionic conductivity and the lattice parameter.[17] These compounds can be classified into five series of solid solutions, (A) $(La_{1-x}Nd_x)_{0.56}Li_{0.33}TiO_3$, (B) $La_{0.56}Li_{0.33}M^{4+}{}_xTi_{1-x}O_3$ ($M^{4+}$ = Zr, Hf), (C) $(Ca_{1-x}Sr_x)_{0.56}Li_{0.33}Ta_{0.56}Ti_{0.44}O_3$, (D) $(Ca_{1-x}Sr_x)_{0.56}Li_{0.33}Fe_{0.225}Ta_{0.775}O_3$, and (E) $Sr_{0.56}Li_{0.33}M^{3+}{}_{0.225}Ta_{0.775}O_3$ ($M^{3+}$ = Cr, Fe, Co, Ga, Y). The variations in ionic conductivity can also be divided into two groups, one group composed of the series (A) and (B) containing only tetravalent ions in the B-site and the other composed of the series (C), (D), and (E) containing the Ta ion in the B-site. The ionic conductivity was found to reach a maximum at 0.387 and 0.395 nm, respectively, for the two groups. These results also suggest that to realize high Li ion conductivity for the compound containing a pentavalent cation in the B-site, a relatively larger lattice is required.

It is, however, well-known that the Ti−O bond of perovskite titanates does not have a completely ionic character. Courths et al. have carried out photoemission measurements for $SrTiO_3$,[20] finding a hybridization between the Ti 3d and the O 2p states and an estimated ionic charge of the Ti ion of +2.5. Furthermore, the net charge of Ti ion in the $(TiO_6)^{8-}$ cluster in $SrTiO_3$ was estimated at +2.44 based on a molecular orbital calculation using the DV-Xα cluster method.[21] By the photoemission study of a single crystal of $BaTiO_3$, the covalent character of the Ti−O bond was confirmed in the cubic and tetragonal phases and the static charges of the Ti ion were predicted to be reduced from the formal charge.[22] Considering these results, the Ti−O bond of $La_{2/3-x}Li_{3x}TiO_3$, which is one of the perovskite titanates, must have covalent character.

Even though this reduction of the valence of the Ti ion from the formal charge has been predicted by various studies, the covalent character of the Ti−O bond has not been taken into account in previous research regarding perovskite-type Li ion conductors. Hence, we attempted in the present study to elucidate the influence of the Ti−O bond's covalent character on Li ion conduction using a molecular dynamics simulation (MD). The MD is a very useful method for such an investigation because it allows us to easily change the chemical factor, that is, the covalent character, for each bond. In this study, the MD was carried out using two different potential models, a fully ionic model (FIM) and a partially ionic model (PIM), and the reproducibility of the physical properties and the Li ion conduction were compared.

**Table 1. Potential Parameters for FIM**

| ion | number of ions | $z$ | $a$ (nm) | $b$ (nm) | $c \times 10^3$ ($kJ^{-1/2}\cdot nm^3\cdot mol^{-1/2}$) |
|---|---|---|---|---|---|
| O | 540 | −2.000 | 0.1750 | 0.012 | 84 |
| Ti | 180 | +3.000 | 0.1293 | 0.008 | 0 |
| La | 108 | +3.000 | 0.1707 | 0.010 | 29 |
| Li | 36 | +1.000 | 0.1034 | 0.008 | 8 |

## Experimental Section

**Experimental Procedure.** A $La_{0.6}Li_{0.2}TiO_3$ polycrystalline sample for the investigation of physical properties and structure was prepared by the conventional solid-state reaction technique. Powders of $La_2O_3$ (99.9%), $Li_2CO_3$ (99.9%), and $TiO_2$ (99.9%) were used as the starting materials. The mixture was calcined at 1373 K for 12 h, sintered at 1423 K for 5 h, and quenched to room temperature so that the arrangement of lanthanum ions was in the disordered state. Thermal expansion was measured using a high-temperature X-ray diffractometer (Mac Science MXP[18] X-ray diffractometer) from 300 to 1200 K. The Li ion conductivity was measured by the ac impedance method using an HP 4192 impedance analyzer in the frequency range of 5 Hz to 13 MHz.

**Simulation Procedure.** A simulation cell has 180 perovskite unit cells ($a \times b \times c = 6 \times 6 \times 5$) in which La, Li, and vacancy are distributed randomly among the A-sites. The numbers of each ion are shown in Table 1. Periodic boundary conditions were used for the simulation cell. Simulations were executed using the program MXDORTO developed by Kawamura.[23] This program achieved a rapid convergence by the Ewald method and applied the Verlet algorithm[24] for the motion of atoms. In this simulation, the temperature and pressure were controlled by the scaling of particle velocities and basic cell parameters, respectively.[25] For all simulations, the integration time was 2 fs. The initial aging was carried out in 150000 steps for each model. After the calculation of 50000 steps under constant temperature and volume, the 100000 steps were executed under constant temperature and pressure.

The interatomic potential of the FIM is expressed by

$$U_{ij} = \frac{z_i z_j e^2}{r_{ij}} + f_0(b_i + b_j)\exp\left[\frac{(a_i + a_j - r_{ij})}{(b_i + b_j)}\right] - \frac{c_i c_j}{r_{ij}} \quad (1)$$

The first term in eq 1 represents a Coulomb interaction where $z_i$ and $z_j$ are effective charges of the ions $i$ and $j$, respectively, and $r_{ij}$ is the interatomic distance between the ions.[26] In the FIM, each bond is assumed to be fully ionic; thus, the effective charge is equal to the formal charge of each ion. The second term represents the short-range repulsion potential. The parameters $a_i$ and $a_j$ reflect the radius, and $b_i$ and $b_j$ reflect the hardness of ions $i$ and $j$, respectively. The quantity $f_0$ is a constant $6.9478 \times 10^{-11}$ N. The third term represents the dipole−induced dipole dispersion potential based on the van der Waals interaction. The specific parameters of each ion, $a_i$, $b_i$, and $c_i$, were determined by the trial and error method. The optimized parameters are given in Table 1.

In the PIM, the interatomic potential is given by the following,

$$U_{ij} = \frac{z_i z_j e^2}{r_{ij}} + f_0(b_i + b_j)\exp\left[\frac{(a_i + a_j - r_{ij})}{(b_i + b_j)}\right] - \frac{c_i c_j}{r_{ij}} + F_{ij}\{\exp[-2\beta_{ij}(r_{ij} - r^*_{ij})] - 2\exp\{-\beta_{ij}(r_{ij} - r^*_{ij})]\} \quad (2)$$

(20) Courths, R.; Cord, B.; Saalfeld, H. *Solid State Commun.* **1989**, *70*, 1047−1051.
(21) Tsukada, M.; Satoko, C.; Adachi, H. *J. Phys. Soc. Jpn.* **1980**, *48*, 200−210.
(22) Hudson, L. T.; Kurtz, R. L.; Robey, S. W.; Temple, D.; Stockbauer, R. L. *Phys. Rev. B* **1993**, *15*, 1174−1180.
(23) Kawamura, K. MXDORTO, Japan Chemistry Program Exchange, #029.
(24) Verlet, L. *Phys. Rev.* **1964**, *159*, 98−103.
(25) Woodcock, L. V. *In Advanced Molten Salt Chemistry*; Plenum: New York, 1975.
(26) Kawamura, K. *Proc. 13th Taniguchi Symp., Kashikojima Japan* **1990**, No. 6, 87−97.

**Table 2. Potential Parameters for PIM**

| ion | number of ions | $z$ | $a$ (nm) | $b$ (nm) | $c \times 10^3$ (kJ$^{-1/2}$·nm$^3$·mol$^{-1/2}$) |
|---|---|---|---|---|---|
| O | 540 | −1.267 | 0.19265 | 0.018 | 84 |
| Ti | 180 | +2.400 | 0.11158 | 0.010 | 0 |
| La | 108 | +2.000 | 0.17070 | 0.010 | 29 |
| Li | 36 | +1.000 | 0.10010 | 0.008 | 8 |

| ion pair | $F_{ij}$ (kJ·mol$^{-1}$) | $\beta$ (nm) | $r^*$ (nm) |
|---|---|---|---|
| Ti−O | 260 | 20 | 0.188 |

The physical meaning of the former three terms of eq 2 is the same as that of eq 1.[26] However, the effective charge of ions $z_i$ and $z_j$ of the PIM is different from that of the FIM. In the PIM, the effective charge is reduced from the formal charge in consideration of the influence of the covalent character. Kim et al. have executed the MD using the PIM for $TiO_2$ polymorphs (brookite, anatase, and rutile).[27] In their simulation, the contribution of the ionic bond in the Ti−O bond was assumed to be 60%; that is, the effective charge of the Ti ion was determined to be +2.4. As a result, crystal structures and physical properties, including the thermal expansion and bulk modulus, of these polymorphs were reproduced very well. The validity of these values was also supported by several studies of $SrTiO_3$, which has a similar crystal structure to that of $La_{0.6}Li_{0.2}TiO_3$. According to the band calculation based on the augment plane wave function for $SrTiO_3$, the number of d electrons in the Ti muffin-tin sphere was estimated to be 1.48 per Ti ion.[28] Since the dispersion curve of the electronic band structure of this calculation was in good agreement with the results of the angle-resolved photoemission study,[29] this value can be considered to be sufficiently reliable. On the basis of the angle-integrate photoemission experiment for $SrTiO_3$ single crystal, the number of d electrons in the Ti ion was estimated to be 1.5, which implies that the effective charge of the Ti ion is +2.5.[20] Accordingly, these values were used as the effective charge of the Ti ion in this simulation. The effective charge of the La ion is reduced from formal charge +3.0 to +2.0 because the ionicity of the La−O bond calculated from the difference in electron negativities between O and La ions is approximately 75%.[30] The effective charge of the Li ion was found to be constant, the normal valence being +1.0. The effective charge of the O ion was determined to be −1.274 to maintain the charge neutralization. The last term of eq 2 represents the Morse potential where the directionality is ignored. In this simulation, the parameters $F_{ij}$, $\beta_{ij}$, and $r^*_{ij}$ were applied only for Ti and O ions, and the values used in a previous study of $TiO_2$ polymorphs[27] were adopted. Other potential parameters were determined by the trial and error method to reproduce the compressibility, thermal expansion, and structure. All the parameters using the PIM are listed in Table 2.

The diffusion coefficient was calculated from the time dependence of the mean square displacement (MSD), $\langle \Delta r(t)^2 \rangle$, using the Einstein relation

$$\langle \Delta r(t)^2 \rangle = A + 6Dt \tag{3}$$

where $A$ is a constant. The period of the simulation for the estimation of the diffusion coefficient was 200 ps (100000 steps). The ion conductivity, $\sigma$, was calculated from $D$ using the Nernst−Einstein equation,

$$\sigma = \frac{Dcze^2}{kT} \tag{4}$$

where $c$ and $z$ are the carrier concentration and the valence of the mobile ion, respectively. The pair correlation function, $g_{ij}(r)$, is expressed as follows,

$$g_{ij}(r) = \sum_j^{N_j} \frac{n_{ij}(r - \Delta r/2; r + \Delta r/2)}{4\pi(N_i N_j/V) r^2 \Delta r} \tag{5}$$

where $V$ is the volume of the simulation cell and $N_i$ and $N_j$ are the number of ions $i$ and $j$ in this cell, respectively. The $n_{ij}$ term represents the number of ions $j$ in the area between sphere 1 (its radius is $r - \Delta r$) and sphere 2 (its radius is $r + \Delta r$), whose center is ion $i$. In this study, $\Delta r$ is 0.001 nm. The number of ions $j$ in the sphere whose center ion $i$ and radius is $r'$, $n_{ij}$, expresses the coordination number of ion $j$ within the distance $r'$ and is related to $g_{ij}(r)$ by the following equation:

$$n_{ij}(r') = \frac{4\pi N_j}{V} \int_0^{r'} g_{ij}(r) r^2 \, dr \tag{6}$$

**Table 3. Lattice Parameters as Obtained by MD Simulation and Experimental Results**

| | PIM | FIM | exp. |
|---|---|---|---|
| $a_p(=V^{1/3})$ (nm) | 0.387 | 0.3877 | 0.38772(2) |
| $a$ (nm) | 0.391(1) | 0.3883(3) | |
| $b$ (nm) | 0.385(1) | 0.3871(2) | |
| $c$ (nm) | 0.386(1) | 0.3877(3) | |

## Results and Discussion

**Reproducibility of the Crystal Structure and Physical Properties.** Table 3 lists the lattice parameters of the simulation and the experimental. A little distortion was observed in each model. The perovskite parameter (cube root of the unit cell volume), $a_p$, for each model was consistent with the experimental value. While a little crystal distortion was observed, the difference in the cell volume between simulation and experiment was found to be insignificant.

Figure 1 shows the variation in the densities with temperature calculated using the FIM, the PIM, and the experimental results. The bulk thermal expansion coefficients, α, determined by the simulation and experiment are $3.09 \times 10^{-5}$ (PIM), $1.00 \times 10^{-5}$ (FIM), and $2.66 \times 10^{-5}$, respectively. While the α obtained by the FIM was one-third the experimental α, that obtained by the PIM was in good agreement with the experimental value. The thermal expansion is caused by the asymmetry of the interatomic potential. The potential shape of the PIM is more asymmetric than that of the FIM because of the addition of the Morse potential term in eq 4. The good agreement of the PIM with the experimental results proves that the PIM reproduces the shape of the actual interatomic potential.

Figure 2 shows the volume change of $La_{0.6}Li_{0.2}TiO_3$ under hydrostatic pressure as calculated by the MD and the experimental data of the $SrTiO_3$.[31] The initial compressibility, $\kappa$, which was obtained by extrapolation of the linear part of the data in the low-pressure region, is $2.23 \times 10^{-12}$ Pa$^{-1}$ by the FIM and $6.06 \times 10^{-12}$ Pa$^{-1}$ by the PIM. While the data obtained by the PIM are in good agreement with the experimental results for the

(27) Kim, D. W.; Enomoto, N.; Nakagawa, Z.; Kawamura, K. *J. Am. Ceram. Soc.* **1996**, *79*, 1095−1099.
(28) Takegahara, J. *J. Electron. Spectrosc. Relat. Phenom.* **1994**, *66*, 303−320.
(29) Haruyama, Y.; Kodaira, S.; Aiura, Y.; Bando, H.; Maruyama, T.; Sakisaka, Y.; Kato, H. *Phys. Rev. B* **1996**, *53*, 8032−8035.
(30) Pauling, L. *The Nature of Chemical Bond*; Cornell University Press: New York, 1960.
(31) Edwards, L. R.; Lynch, R. W. *J. Phys. Chem. Solids* **1970**, *21*, 573−574.

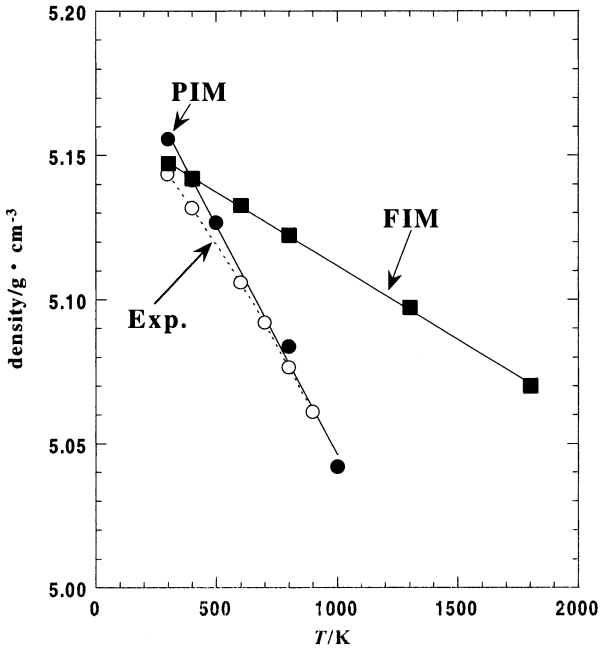


**Figure 1.** Temperature dependence of density for $La_{0.6}Li_{0.2}TiO_3$ in the PIM, FIM, and experiment.

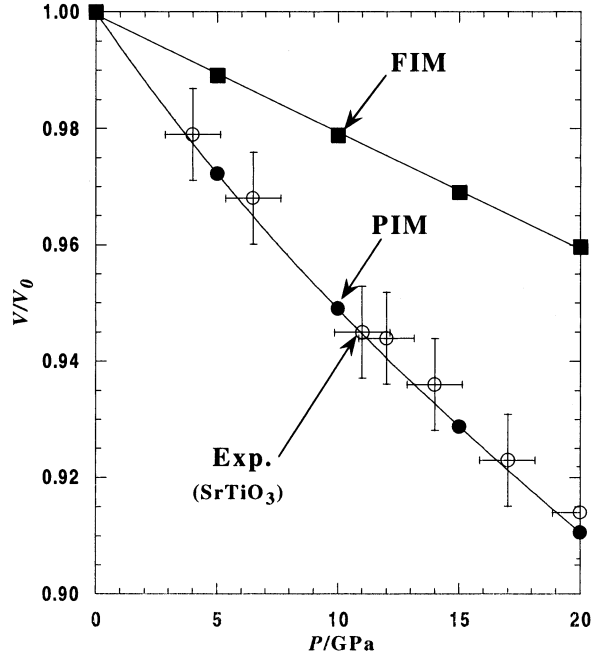


**Figure 2.** Variations in relative cell volume with pressure of $La_{0.6}Li_{0.2}TiO_3$ obtained by MD using the FIM and PIM and experiment for $SrTiO_3$.[29]

$SrTiO_3$, the FIM values are smaller than those of the PIM. The large difference in $\kappa$s between the two potential models is probably caused by the difference in the effective charges between the PIM and the FIM. For the PIM, the effective charges were reduced from normal charges; thus, the Coulomb attractive force in the FIM is stronger than that of the PIM. The Coulomb attractive force in the FIM is so strong that the ions of the FIM are harder to maintain in the same structure as in the PIM. Therefore, the compressibility of the FIM is reduced. The good agreement of the compressibility of the PIM with the experimental results for $SrTiO_3$ indicates that the bond strength is more actually reproduced by the PIM.

**Position of Li Ions.** While many efforts have been expended to determine the crystal structure of (La,Li)-$TiO_3$, there are still controversies over it, especially the Li ion location. According to the neutron-diffraction experiments, it was indicated that the Li ions located in the center of the A-site, the off-center position, and the bottleneck position for $La_{0.56}Li_{0.32}TiO_3$, $La_{0.62}Li_{0.16}$-$TiO_3$, and $La_{0.5}Li_{0.5}TiO_3$, respectively.[32−34] On the other hand, the displacement of Li ions from the center of the A-site has been suggested by the simple energy calculation,[10] the NMR study of the (La,Li)$TiO_3$.[18] In this study, an attempt at using the MD to predict a stable position for the Li ion was made.

Figure 3 shows a trajectory plot of the [100] plane at 300 K for the FIM and the PIM. As shown, Li ions displaced from center of the A-site and some Li ions migrate from one A-site to another over the bottleneck. In a comparison of plots between the FIM and the PIM, Li ions were found to be more active with the PIM. To investigate the position of Li ions in more detail, the pair correlation function was calculated for the FIM and PIM.

Figure 4 shows the pair correlation function, $g(r)$, for the FIM and PIM. In both models, the peaks of $g_{O-Ti}(r)$, $g_{Ti-Ti}(r)$, and $g_{La-Ti}(r)$ can be observed at approximately 0.19, 0.39, and 0.34 nm, respectively, which is consistent with the bond lengths in the actual compound. The peak shapes of $g_{Li-Ti}(r)$ and $g_{La-Ti}(r)$ are almost the same between the FIM and PIM. For the peaks of $g_{O-Ti}(r)$ and $g_{Ti-Ti}(r)$, however, a distinguishable difference can be observed; that is, the peak of the PIM is broader than that of the FIM. Two reasons for this peak broadening are considered herein. One is that PIM allows for wide range of stable positions for Ti and O ions in the simulation cell. Another reason is that the thermal vibration of Ti and O ions is larger with the PIM. While we cannot determine which factor is dominant by these data, the latter reason seems to be valid, as a larger thermal expansion was observed with the PIM.

The position of the $g_{Li-Ti}(r)$ peak was different from that of the $g_{La-Ti}(r)$ peak and the first peak overlapped with the second peak for $g_{Li-Ti}(r)$. These results suggest that the Li ions mainly resided in an off-center position and moved actively in the area vicinity of this off-center position. The first and second peaks were observed at approximately 0.28 and 0.40 nm, respectively. Assuming that the direction of the displacement is ⟨100⟩, the distance from the next-nearest-neighbor Ti ion to the Li ion is calculated as 0.42 nm when the distance from the nearest-neighbor Ti ion is 0.28 nm. In the same way, the distance from the next-nearest-neighbor Ti ion to the Li ion is calculated as 0.34 nm if the direction of the displacement is ⟨110⟩. Hence, it is valid that the Li ion was displaced 0.13 nm from the A-site along the ⟨100⟩ direction. The atomic distances calculated from these results are shown in Figure 5.

Figure 6 shows the variations of $g_{Li-O}(r)$ and $n_{Li-O}(r)$ with distance for the PIM and FIM. Comparing figures between the FIM and PIM, the $g_{Li-O}(r)$ of the PIM is

(32) Ruiz, A. I.; López, M. L.; Veiga, M. L.; Pico, C. *J. Solid State Chem.* **1999**, *148*, *329*−*332*.
(33) Inaguma, Y.; Katsumata, T.; Itoh, M.; Morii, Y. *J. Solid State Chem.* **2002**, *166*, 67−72.
(34) Alonso, A.; Sanz, J.; Santamaría, J.; Léon, C.; Váres, A.; Fernández-Díaz, M. D. *Angew. Chem., Int. Ed.* **2000**, *39*, 619−621.

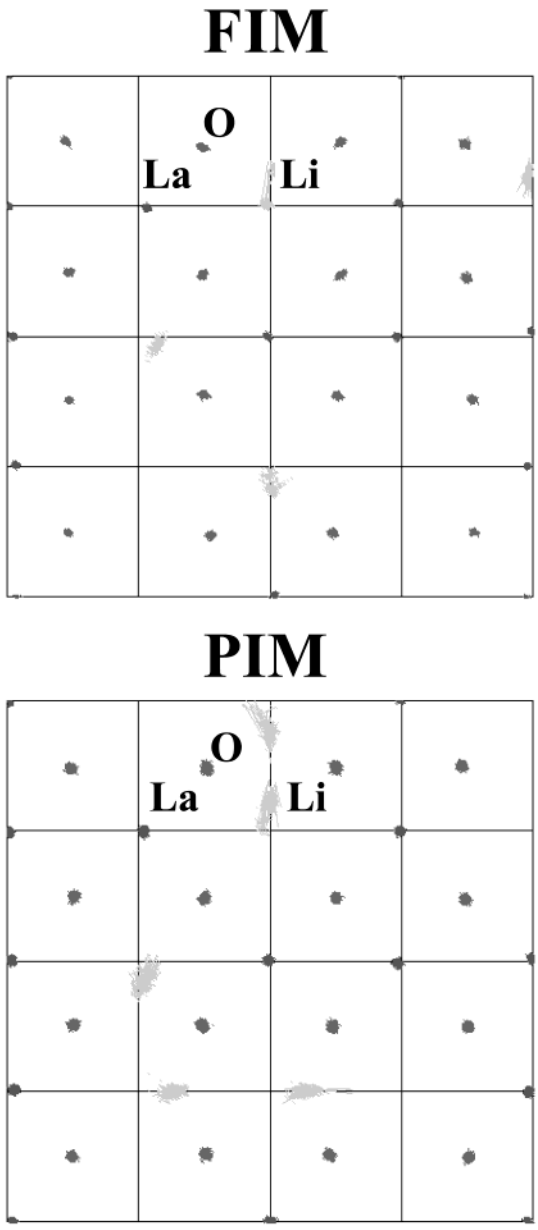


**Figure 3.** Trajectory plots of Li, La, and O ions on the [100] plane for $La_{0.6}Li_{0.2}TiO_3$ at 300 K for the FIM (upper figure) and PIM (lower figure). The line shows the perovskite unit cell.

broader and the $n_{Li-O}(r)$ increases more continuously. The Li ion seems to be spread more widely in the area around the off-center position in the PIM. For the $g_{Li-O}(r)$, the peaks can be observed at 0.20 nm and in the vicinity of 0.30 nm, which is consistent with the calculated values represented in Figure 5. The $n_{Li-O}(r)$ reached approximately 4 at 0.25 nm, which is the end of the first peak of $g_{Li-O}(r)$, and 10 at 0.35 nm, which is the end of the second peak of $g_{Li-O}(r)$ nm. Furthermore, a step can be observed at $n_{Li-O}(r) = 4$, even though it is ambiguous. If the Li ion was displaced in the ⟨100⟩ direction, the $n_{Li-O}(r)$ would reach 4 at the end of the first peak and 8 at the end of the second peak of $g_{Li-O}(r)$. In contrast, assuming that the Li ion was displaced in the ⟨110⟩ direction, the $n_{Li-O}(r)$ would reach 1 at the end of the first peak and 5 at the end of the second peak of $g_{Li-O}(r)$. These results also support that the Li ion was displaced in the ⟨100⟩ direction.

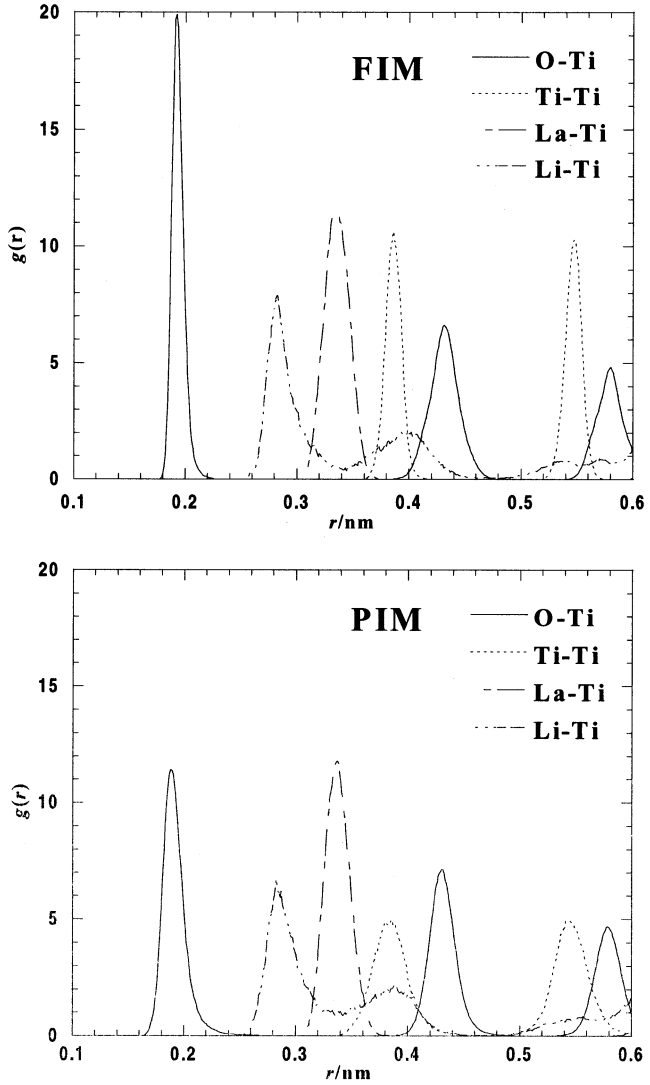


**Figure 4.** Pair correlation functions, $g(r)$, for O−Ti, Ti−Ti, La−Ti, and Li−Ti for the FIM (upper figure) and PIM (lower figure).

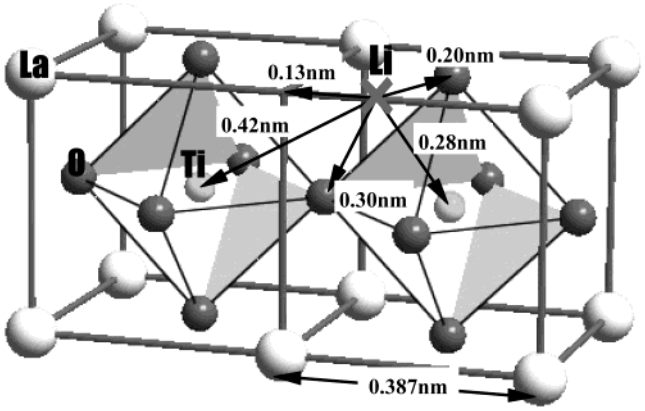


**Figure 5.** Illustration of crystal structure calculated by the pair correlation function. The cross represents the calculated position of the Li ion assuming that the Li ion displaces in the ⟨100⟩ direction. The numbers represent the distance from this position to other ions and the center of the A-site.

Comparing with the experimental data, the displacement of Li ion is also indicated for the close composition compound, $La_{0.62}Li_{0.16}TiO_3$. Inaguma et al. refined the structure of $La_{0.62}Li_{0.16}TiO_3$ by the Rietveld method using neutron-diffraction data.[33] As a result, the position

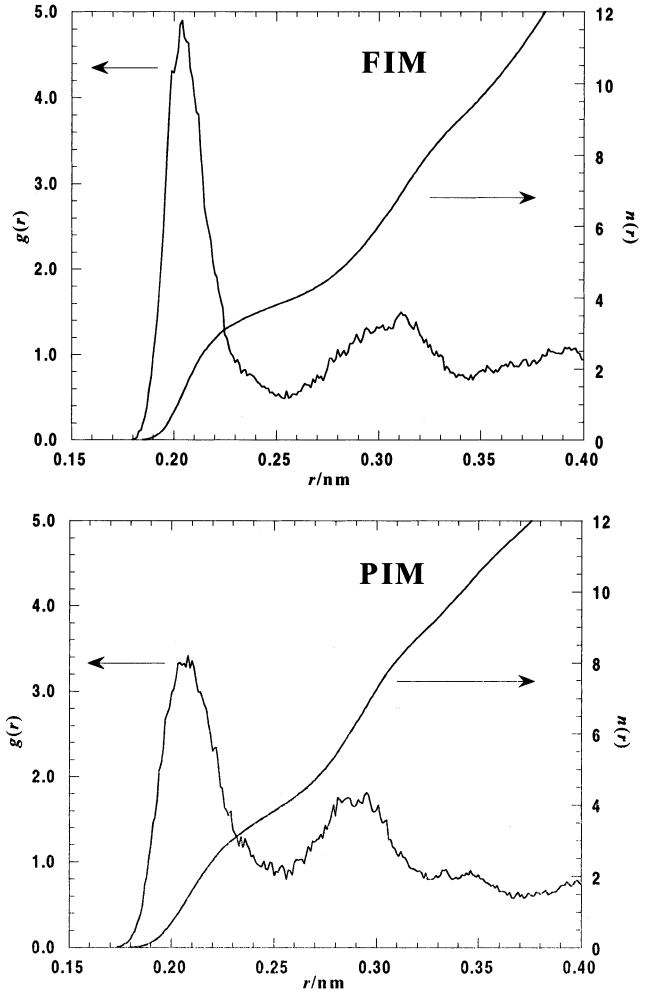


**Figure 6.** Pair correlation function, $g(r)$, and running coordination function, $n(r)$, of the Li−O ion pair for the FIM (upper figure) and PIM (lower figure).

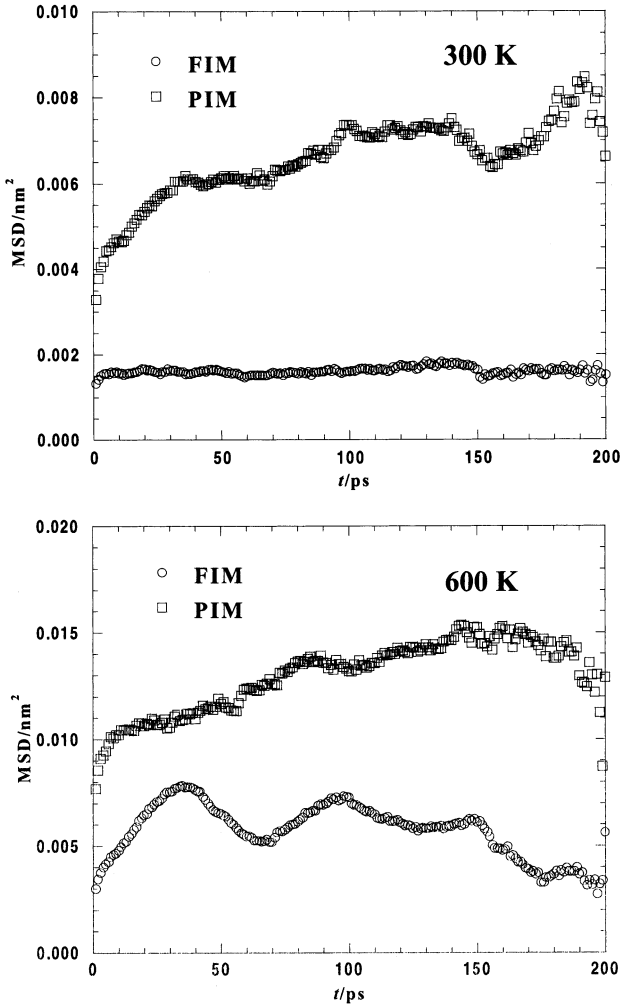


**Figure 7.** Time dependence of the mean square displacement (MSD) of the Li ion for the PIM and FIM at 300 K (upper figure) and 600 K (lower figure).

of the Li ion was refined to be off-centered and in two equivalent positions in the vicinity of the bottleneck. Therefore, it is considered that the position of Li ion in (La,Li)$TiO_3$ depends on the Li composition and the Li ions locate at the off-center position for compounds having close composition to $La_{0.6}Li_{0.2}TiO_3$.

**Influence of Covalent Character on Li Ion Conduction.** In this section, the influence of covalent character on Li ion conduction is elucidated by comparing the Li ion diffusion between the FIM and PIM. Figure 7 shows the time dependence of the MSD of Li ions at 300 and 600 K for the FIM and PIM. While the MSD of the PIM increased with time at 300 K, the MSD of the FIM did not increase with time even at 600 K. These results suggest that the Li ion did not diffuse even at 600 K in the FIM, but diffused at 300 K in the PIM under this simulation condition. According to the pair correlation functions, displacement of Li ion was confirmed for both models. Displacement of the Li ion seems to be responsible for the size mismatch between the Li ion and the La ion. The observation of Li ion conduction in the PIM suggests that the high ion conduction does not occur only as a result of introducing a smaller mobile ion into the A-site.

Figure 8 shows the time dependence of the MSD at 300, 600, and 1000 K for the PIM and at 1000 K for FIM. The diffusion coefficient was calculated from the

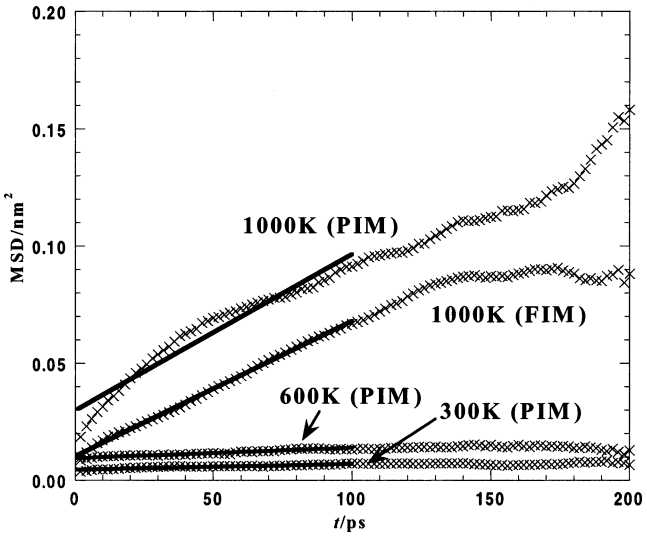


**Figure 8.** Time dependence of the mean square displacement (MSD) of the Li ion at 300, 600, and 1000 K for the PIM and FIM.

slope of this figure in the range from 0 to 100 ps. Table 4 lists the diffusion coefficients and ionic conductivity of the Li ion obtained from the MD and experiment results for 300, 400, 600, and 1000 K. The ionic conductivity obtained by the MD was smaller than the

**Table 4. Diffusion Coefficient and Li Ion Conductivity Obtained by MD and Experiment**

| | $D$ ($cm^2 \cdot s^{-1}$) | | $\sigma$ ($S \cdot cm^{-1}$) | | |
|---|---|---|---|---|---|
| $T$ (K) | FIM | PIM | FIM | PIM | exp. |
| 300 | | $4.07 \times 10^{-8}$ | | $8.67 \times 10^{-4}$ | $1.9 \times 10^{-4}$ |
| 400 | | $4.12 \times 10^{-8}$ | | $6.56 \times 10^{-4}$ | $4.3 \times 10^{-3}$ |
| 600 | | $7.55 \times 10^{-8}$ | | $7.97 \times 10^{-4}$ | $5.0 \times 10^{-2}$ (625 K) |
| 1000 | $9.63 \times 10^{-7}$ | $1.11 \times 10^{-6}$ | $1.01 \times 10^{-2}$ | $1.17 \times 10^{-2}$ | |

experimental value in this temperature range. The diffusion coefficient at room temperature was also smaller than the chemical diffusion coefficient of $La_{0.57}Li_{0.29+\delta}TiO_3$, which were in the range $10^{-6.5}$ to $10^{-7}$ $cm^2/s$, measured by a GITT method.[14] While good linearity of the time dependence of the MSD was not observed in this simulation, this disagreement may not be responsible for the insufficient time span and the number of particles. Even though good linearity was obtained with regard to the time dependence of the MSD in the simulation cell composed by 512 perovskite unit cells, the diffusion coefficient was not consistent with the experimental value. In this simulation, the reproducibility of the diffusion coefficient was found to be influenced by another factor, that is, the arrangement of vacancies, La ions, and Li ions in the A-site. In fact, a different diffusion coefficient was obtained for the simulation cell having a different arrangement of A-site ions and vacancies.[15] Therefore, to obtain the diffusion coefficient more precisely, it may be necessary to determine the most suitable arrangement of A-site ions and to estimate the diffusion coefficient with such an arrangement.

The active diffusion in the PIM is thought to be caused by several factors. One is the reduction of effective charges, which promotes Li ion conduction by several mechanisms. One of these mechanisms is to directly shallow the interatomic potential. The decrease in effective charges shallows the interatomic potential due to the small Coulomb potential. Consequently, Li ions can move more freely in the PIM. The migration of Li ions is also promoted by a softening of the framework ions. In this simulation, the bulk compressibility of the PIM was larger. The weak Coulomb attractive force caused by decreasing the effective charge softens the framework ions and also promotes the Li ion migration. The larger thermal expansion for the PIM due to the addition of the Morse potential term is thought to caused the high Li ion conduction of the PIM at higher temperatures. The expansion of the crystal lattice increases the bottleneck size and promotes the migration of Li ions.

## Conclusion

In a comparison of the reproducibility of physical properties between the FIM and PIM, it was found that good agreement with experimental results can be obtained with the PIM. Our results demonstrate that the PIM is a very effective model for the simulation of such perovskite-type titanates. While displacement of the Li ion in the ⟨100⟩ direction from the center of the A-site was predicted in both models, diffusion of the Li ion was observed only for the PIM below 600 K, suggesting that the introduction of a small mobile ion into the A-site does not always induce high ion conduction and that the covalent character of the Ti−O bond is indispensable for the high Li ion conduction. The MD using the PIM could not quantitatively reproduce the diffusion coefficient, which was caused by the random distribution of the Li ion, La ion, and the vacancy.

**Acknowledgment.** The authors wish to express their thanks for the Grant-in Aid for Scientific Research in the priority area “Dynamics of the Fast Ion Migration in Solid and its Development to Ionics” No. 07239213. Special thanks are also due to Dr. Dae-Weon Kim for his many useful suggestions.

CM0203969